Diamantidis and Haas
Earth, Planets and Space (2023) 75:114
https://doi.org/10.1186/s40623-023-01872-x

Earth, Planets and Space

FULL PAPER

Open Access

Evaluation of the first three years of Vgos 24 h sessions using a Kalman filter with C5++

Periklis-Konstantinos Diamantidis[1*] and Rüdiger Haas[1]

Abstract

We analyzed the first three years of VGOS 24 h sessions, and evaluated the performance in terms of Earth orientation parameters (EOP) and station positions. We estimated radio source coordinates which might be of particular importance in VGOS due to the different observing frequencies compared to legacy S/X VLBI. We investigated the impact of this procedure in the determination of the celestial reference, and detected possible increased crosstalk between radio source positions and nutation. We, thus, created an updated source coordinate catalogue that contains information from the VGOS observations and utilized that as our a priori for further analysis. We found that this procedure significantly attenuates mean biases in the estimated EOP time series. We then utilized a kalman filter with an empirically tuned stochastic modelling for nutation and polar motion and estimated repeatabilities on the 60–80 μ as level for nutation, and 100–130 μ as level for polar motion. The station position repeatabilities were evaluated to be 1.80 and 2.12 mm for the east and north components and 3.98 mm for the vertical, while the baseline length repeatabilities were estimated to be 4.22 mm at 6000 km. These results are promising with respect to the expected future VGOS performance, while increased attention should be paid to the celestial frame determination in the VGOS observing bands.

Keywords VGOS, VLBI, c5++, Kalman filter, EOP, TRF, Nutation, Radio source positions

Graphical Abstract

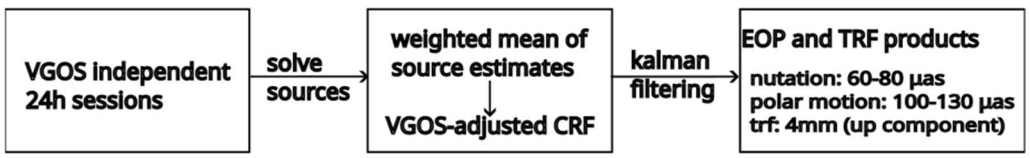

Introduction

Both society at large and the scientific community require a precise and accurate global geodetic reference frame (GGRF). A few years ago, the United Nations adopted a corresponding resolution (UN 2015) and highlighted the importance of a GGRF for a sustainable development. A GGRF is realized as the International Terrestrial Reference Frame (ITRF) (Altamimi et al. 2023) by combining different space-geodetic techniques that are co-located at so-called geodetic core (fundamental) sites. The ideal design of a geodetic core site is described in, e.g., Pearlman et al. (2015). Such a site involves a number of instruments for space-geodetic techniques such as geodetic Very Long Baseline Interferometry (VLBI), Global

*Correspondence:
Periklis-Konstantinos Diamantidis
periklis.diamantidis@chalmers.se
[1] Chalmers University of Technology, Gothenburg, Sweden

Navigation Satellite Systems (GNSS), Satellite Laser Ranging (SLR), and Doppler Orbitography Radiopositioning Integrated by Satellite (DORIS) in close vicinity. The geometrical relations between those instruments, the so-called local ties, should also be determined and monitored with high accuracy in a local survey network that includes a central geodetic marker. These core sites form the backbone of the ITRF and the Global Geodetic Observing System (GGOS) (Plag et al. 2009). In order to fulfill the GGOS goals regarding the accuracy and stability of the derived geodetic products, a new generation of VLBI stations, the VLBI Global Observing System (VGOS) stations are being rolled out with the intention of achieving mm-level accuracy and continuous 24 h observations (Elosegui et al. 2018). Although the continuity in observations has not been yet realized, a significant number of individual VGOS sessions have been performed over the past few years ranging from 1 h intensive sessions involving 1 to 3 baselines, e.g., the so-called VGOS-2 and VGOS-B, to 24 h sessions consisting of several baselines, the VGOS-O. While initial studies in terms of the rapid UT1-UTC determination have already been performed for the intensive sessions (Haas et al. 2021; Diamantidis et al. 2022), the VGOS-O sessions that are sensitive to a wider range of observables are now starting to be evaluated. These 24 h observations need precise a priori information regarding station positions and velocities to avoid significant noise in the definition of the geodetic datum that propagates in the determination of other parameters of interest like Earth orientation parameters (EOP). Until recently this information had to be determined first, through, e.g., a series of short-baseline interferometry measurements (Varenius et al. 2021), or an unconstrained analysis of sessions that contain the state-of-the-art VGOS network (Mikschi et al. 2021). The newest iteration of the ITRF, the ITRF2020 (?), is the first combined catalogue of stations that incorporates the VGOS network, in a homogeneous and consistent way utilizing data from all co-located space geodetic techniques as well as the local ties between them. The increased number of observations of VGOS compared to the legacy S/X VLBI, owing to the shorter integration times and faster-slewing rates, allows a more dense and diverse mapping of the atmosphere. This motivates the use of sophisticated noise models that, e.g., a kalman filter offers for the determination of the tropospheric parameters.

We focused our analysis on estimating station position and EOP repeatabilities using the ITRF2020 for the VGOS-O sessions covering three years, from 2019 through 2021, and evaluated our implementation of a kalman filter (KF) module that works in tandem with the c5++ multi-technique space-geodetic software. Analyses using the same 3-year dataset have already been performed, and showed that radio source position estimates can deviate from the ICRF3 catalogue (Glomsda et al. 2023), and that biases as well as increased EOP repeatabilities appear in VGOS EOP estimates compared to legacy S/X (Glomsda et al. 2023; Nilsson et al. 2023). Using this a basic assumption, we investigated scenarios of formulating VGOS-adjusted radio source catalogues, and studied their effect on EOP estimates in terms of formal errors, mean biases and weighted root mean square (WRMS) metrics. We also studied the behavior of the resulting CRF frame-defining parameters, and radio source coordinate repeatabilities. This approach led us to elect a particular VGOS-adjusted radio source catalogue, which we used in tandem with stochastic modelling of the nutation and polar motion parameters for our final analysis. The effects of these different analysis options in terms of EOP, station position, and baseline length repeatabilities were also determined.

The *Methods* section introduces the dataset used in the analysis, discusses various aspects of the KF implementation, as well as the parameterization and the different solutions that were performed. The *Results and Discussion* section shows the station position repeatabilities obtained from the KF implementation, and the EOP estimation process and the derived products. Finally, the *Conclusions* section provides the reader with the summary and conclusions, and outlines future work concerning this topic.

Methods

Input data

A total of 72 daily (24 h) observation sessions of the VGOS network from 2019 to 2021 were used in this analysis. These include all sessions with 5 stations or more. The data were obtained in the vgosDb format (Bolotin et al. 2015) from the CDDIS data server (Noll 2010). The participating stations and their positions are shown in Fig. 1. These stations are not present in all the sessions, e.g., Mg became operational after mid-2019. The percentage of the sessions that were performed with respect to the number of participating stations is presented in Table . 1.

Kalman filter and space-geodetic techniques

Kalman filtering has been already applied to the analysis of geodetic VLBI and GPS data (Herring et al. 1990; Nilsson et al. 2015; Soja et al. 2015; Karbon et al. 2017; Webb and Zumberge 1995). In summary, this recursive estimation technique is based upon a combination of a linear model of the time evolution of a state vector, x_{t_i}, at epoch t_i, as described by

$$x_{t_i} = A_{t_i} x_{t_{i-1}} + w_{t_i}, \tag{1}$$

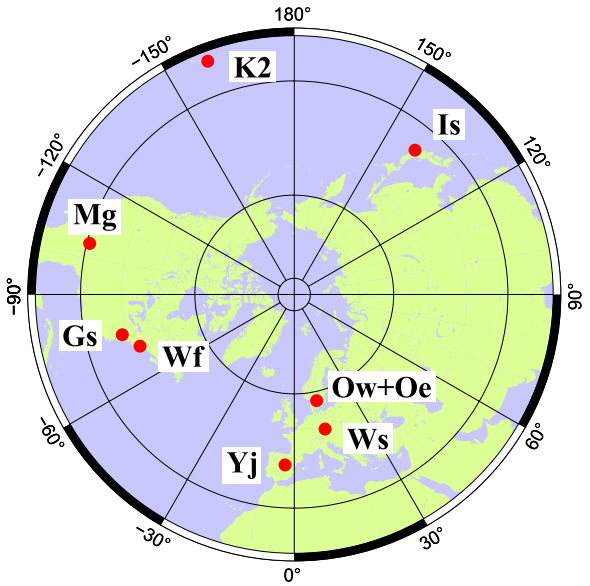

Fig. 1 The radio telescopes of the VGOS network that took part in 24 h observation sessions 2019–2021. These include the telescopes located in Onsala (Ow+Oe, Sweden), Ishioka (Is, Japan), Wettzell (Ws, Germany), Yebes (Yj, Spain), Westford (Wf, USA), Kokee Park (K2, USA), and the ones at the Goddard Geophysical and Astronomical Observatory (Gs, USA), and the McDonald Observatory (Mg, USA)

Table 1 The percentage of sessions in relation to the number of stations that participated

Nr. of stations	% of sessions
5	16.6
6	23.6
7	37.5
8	12.5
9	9.8

where A_{t_i} is the state transition matrix and w_{t_i} is the process noise, with observations, z_{t_i}. The latter can infer the state vector via the linear model

$$z_{t_i} = H_{t_i} x_{t_i} + v_{t_i}, \tag{2}$$

where H_{t_i} is the observation matrix and v_{t_i} the observation noise. The optimal a posteriori estimate of the state vector, $\hat{x}_{t_i|t_i}$, at epoch t_i, can then be retrieved via

$$\begin{aligned}\hat{x}_{t_i|t_i} =& \hat{x}_{t_i|t_{i-1}} \\ &+ P_{t_i|t_{i-1}} H_{t_i}^T (H_{t_i} P_{t_i|t_{i-1}} H_{t_i}^T + R_{t_i})^{-1} (z_{t_i} - \hat{z}_{t_i}),\end{aligned} \tag{3}$$

where $\hat{x}_{t_i|t_{i-1}}$ is the a priori estimate of the state vector at epoch t_i, $P_{t_i|t_{i-1}} = \mathbb{E}[(x_{t_i} - \hat{x}_{t_i|t_{i-1}})(x_{t_i} - \hat{x}_{t_i|t_{i-1}})^T]$ the a priori error state variance-covariance matrix and $R_{t_i} = \mathbb{E}[v_{t_i} v_{t_i}^T]$ the variance-covariance matrix of the observation noise. In the case of the space-geodetic techniques the observation equation is non-linear, i.e.,

$$z_{t_i} = h(x_{t_i}, p) + v_{t_i} \tag{4}$$

where p are other constant parameters. This necessitates the use of the extension of the linear KF algorithm to the non-linear filtering problems, the so-called extended KF (EKF). While the detailed derivation on both the KF and the EKF can be found in, e.g., Ribeiro (2004), some key aspects of the filtering process, pertaining to the handling of non-linearities in the observation equation, are presented here.

In the linear case, the a priori estimate of the state vector, $\hat{x}_{t_i|t_{i-1}}$, is transformed into the observation space to obtain the estimated observation, $\hat{z}_{t_i|t_{i-1}}$, by

$$\hat{z}_{t_i|t_{i-1}} = H_{t_i} \hat{x}_{t_i|t_{i-1}}. \tag{5}$$

Using Eq. 2 that contains the true value of the state, x_{t_i} at epoch t_i, and Eq. 5, the variance-covariance matrix of the measurement residual can be constructed as

$$\begin{aligned} S_{t_i} &= \mathbb{E}[(z_{t_i} - \hat{z}_{t_i})(z_{t_i} - \hat{z}_{t_i})^T] \\ &= \mathbb{E}[(H_{t_i}(x_{t_i} - \hat{x}_{t_i|t_{i-1}}) + v_{t_i})(H_{t_i}(x_{t_i} - \hat{x}_{t_i|t_{i-1}}) + v_{t_i})^T] \\ &= H_{t_i} \mathbb{E}[(x_{t_i} - \hat{x}_{t_i|t_{i-1}})(x_{t_i} - \hat{x}_{t_i|t_{i-1}})^T] H_{t_i}^T + \mathbb{E}[v_{t_i} v_{t_i}^T] \\ &= H_{t_i} P_{t_i|t_{i-1}} H_{t_i}^T + R_{t_i}, \end{aligned} \tag{6}$$

the so-called innovation matrix.

In the non-linear case, the procedure described above has to be modified. The observation equation as stated in Eq. 4 is linearized using a first-order Taylor expansion around a linearization point, which in this case is determined by the a priori estimate of the state vector, $\hat{x}_{t_i|t_{i-1}}$, and any parameters used as constant a priori information p,

$$\begin{aligned} z_{t_i} &= h(x_{t_i}, p) + v_{t_i} \\ &= h(\hat{x}_{t_i|t_{i-1}}, p) + \left.\frac{\partial h}{\partial x}\right|_{x=\hat{x}_{t_i|t_{i-1}}} (x_{t_i} - \hat{x}_{t_i|t_{i-1}}) + v_{t_i}. \end{aligned} \tag{7}$$

The estimated observation is retrieved from the non-linear model

$$\hat{z}_{t_i} = h(\hat{x}_{t_i|t_{i-1}}, p). \tag{8}$$

Using Eq. 7 and Eq. 8 in Eq. 6, the innovation matrix S_{t_i} is computed to be identical to the linear case with the exception that H_{t_i} refers now to the Jacobian matrix around the linearization point.

Kalman filter in c5++

The data analysis is carried out using the c5++ analysis software (Hobiger et al. 2010). This software is able to process VLBI, GPS and SLR data individually or in a multi-technique mode where those techniques are combined on the observation level (Hobiger and Otsubo 2014; Hobiger et al. 2014; Hobiger and Otsubo 2017). The software is built for analysis on daily or subsequent daily sessions, but lacks the ability to perform global solutions, i.e., combining sessions that are not time-contiguous. The data processing is routinely carried out with the use of an iterative least-squares (LSQ) adjustment based on the Gauss-Markov model (Koch 1988), including the three-sigma rejection criterion and the possibility of using the variance-component estimation (VCE) within the estimation process (Hobiger and Otsubo 2017). For this analysis, we developed a KF module that works in tandem with c5++ taking advantage of the recursive nature of the algorithm for a smaller computational footprint and the ability to model target states as stochastic processes with input model uncertainty. The module, at present, works for the VLBI and GNSS techniques. The outlier detection and rejection procedure is carried out with the use of a hybrid approach employing the Mahalanobis distance metric and the three-sigma rejection criterion. More specifically, using the innovation matrix S_{t_i} as defined in Eq. 6, the Mahalanobis distance is computed as

$$d_{t_i} = \sqrt{z_r^T S_{t_i}^{-1} z_r}, \tag{9}$$

where $z_r = z_{t_i} - \hat{z}_{t_i}$ is the a priori observation residual. This metric is then used to determine whether an outlier is present in the multivariate observation vector (Chang 2014). If such an event occurs, the three-sigma criterion is employed in the individual elements of the observation vector to detect and discard the outliers. The error state variance-covariance matrix, P_{t_i}, at any epoch t_i must be positive definite for KF to be physically meaningful. This positive definiteness is not guaranteed using the EKF algorithm, and thus a variation of its formulation, the Extended Square-Root Covariance Filter is implemented, see, e.g., Park and Kailath (1995). A forward-backward kalman smoother is applied to make full use of the observation data. This also gives the opportunity for the VCE method already used in LSQ to be adapted for use in the KF by applying a VCE-derived weight from the forward run on the backward run and vice-versa.

Parameterization

In total three main analyses have been performed. One (S1) where the sources were fixed to ICRF3 (Charlot et al. 2020), and two (S2, S3) where the sources were fixed to the VGOS-adjusted ICRF3 source catalogue (VA-ICRF3). We also performed two auxiliary analyses. One (A1) where the radio sources were solved with no contraints on EOP, and one (A2) where the radio sources were solved by imposing constraints on EOP. The VA-ICRF3 we used in S2 and S3 is the weighted mean of the radio sources that were estimated from A2. The comparison of the CRF products generated from A1 and A2 along with details about their specific parameterizations are given in the section *Radio source positions in VGOS*. For all solutions, we used the ITRF2020 (Altamimi et al. 2023) for our a priori station positions and velocities, and the IERS C04-20 series for the a priori EOP. We use the recommendations of the IERS 2010 conventions regarding displacement models and high-frequency EOP, and additionally the post-seismic models present in the ITRF2020 solution. The GPT3 and VMF3 models (Landskron and Böhm 2018) for temperature, pressure and mapping functions for the slant delays were used, respectively. The radio sources were estimated using a module incorporating the MODEST implementation for partials (Sovers et al. 2004) and the no-net-rotation (NNR) constraints as formulated in Jacobs et al. (2010). In the S3 solution, we employed stochastic modelling for nutation and polar motion. In particular, we used a random walk model as proposed by Karbon et al. (2017) and empirically tuned its stochastic characteristics calibrating it so that the resulting formal errors were equivalent to those we computed when we treated them as constant parameters. We ended up with a stochastic noise of 0.0025 mas^2/d for polar motion and 0.00011 mas^2/d for nutation. These values are lower than the ones investigated from Karbon et al. (2017) which were between 0.12−0.02 mas^2/d for polar motion and 0.01 mas^2/d for nutation, but we are estimating the differences to the a priori modelled high-frequency EOP corrections, instead of the high-frequency EOP corrections themselves. It is also the case, that this smaller noise is additionally mitigating the crosstalk between EOP and source coordinates. To test the validity of this parameterization on the particular dataset, we present the effect that this updated EOP determination method has on station position and baseline length repeatabilities. The detailed parameterization options are presented in Table 2.

Results and discussion

We start our analysis by evaluating the significance that radio source position corrections have in our solutions. In particular, we want to establish whether one needs to take into account any systematic effects that do not show up or show up to a significantly lesser extent in, e.g., legacy S/X observations. For a comparison to S/X, see, e.g., Glomsda et al. (2023).

Table 2 Parameterization of the target parameters. ZWD stands for zenith wet delay, and GRN/GRE for north and east gradients. STACLK is the station clock, and STAX are the station positions. Finally the EOP are presented in the form of dX/dY as the celestial pole offsets, and x_p/y_p as polar motion in X and Y. The VA-ICRF3 is produced with solution A2 in a process presented in the section *Radio source positions in VGOS*

Parameter	Parameter type	Stochastic noise		
		S1	S2	S3
ZWD	Random walk	36 mm^2/h		
GRN/GRE	Random walk	0.36 mm^2/h		
STACLK	Integrated random walk	0.64 ns^2/day^3		
STAX	Constant	–		
UT1-UTC	Constant	–		
dX/dY	Constant or random walk	–	–	0.00011 mas^2/day
x_p/y_p	Constant or random walk	–	–	0.0025 mas^2/day
A priori TRF		ITRF2020		
A priori CRF		ICRF3	VA-ICRF3	VA-ICRF3
A priori EOP		IERS-20-C04		
Weighting technique		Baseline-based VCE		

Radio source positions in VGOS

The ICRF3 that we take as our a priori has been determined from S/X observations, however, VGOS is operating on different frequency bands, see, e.g., Niell et al. (2018). Given that radio source positions are frequency-dependent (Xu et al. 2022; de Witt et al. 2022), part of the residual information, after reducing the VGOS observables, may concern possible differences in radio source positions with respect to the a priori. At the same time, radio source positions, and thus the celestial frame definition, is correlated to EOP estimates. A processing strategy using independent daily VGOS sessions may not be enough to de-correlate the estimated parameters when significant corrections exist in the 7-parameter set described above, namely, UT1-UTC, polar motion, nutation, and the right ascension and declination of the sources. In this case, significant leakage can occur between estimates of the correlated parameters, degrading the overall solution. In previous analyses (Haas et al. 2021; Diamantidis et al. 2022), we did not encounter such an effect being present for UT1-UTC, and thus we focus in the following on polar motion and nutation. We illustrate this in Fig. 2 by presenting the formal errors of nutation and polar motion for two different solutions. One where the source positions were fixed to ICRF3 (S1), and one where the source positions were estimated by imposing a NNR condition on the subset of defining sources of the ICRF3 catalogue that have more than 5 observations per session (A1). We can clearly see that estimating radio sources increases the uncertainties for polar motion and nutation approximately by a factor of 0.5 and 5, respectively. This result makes sense, in the context of increased crosstalk, since there is a direct correlation between the celestial frame axes and nutation, and an indirect one with polar motion which is prone to absorbing the diurnal components of nutation, especially if the latter is not estimated (Karbon et al. 2017). In order to mitigate the effect, we decided to combine the daily estimates of the radio source positions, in a VA-ICRF3 to be used as the celestial frame reference in the following independent daily analyses. Firstly, we calculated the weighted mean of the source coordinates as determined from the 72 independent sessions. The resulting source catalogue was then used as a fixed a priori. This solution, identical to S1 except for the a priori CRF, is denoted as S1.5, and the results in terms of mean bias with respect to the C04-20 EOP series are presented in Fig. 5. We see that the updated source catalogue is inducing an alignment effect for polar motion to its a priori mean, something which is particularly visible for the X-component. However, the mean bias of nutation does not seem to be particularly affected. As Fig. 2 indicated, nutation seems to be the most prone to leak into source coordinates, and thus we proceeded to generate a new solution (A2) where we estimate source coordinates but at the same time impose a soft constraint in the form of a priori uncertainty for our nutation and polar motion of 25 μas and 50 μas, respectively. This is done to upweigh source coordinate over nutation corrections in the estimation process. The choice of the level of the constraints is such that this first step will lower the formal errors for nutation and polar motion towards the level they have when radio sources are fixed to ICRF3. The underlying assumption is that, should increased crosstalk exist, it would primarily affect

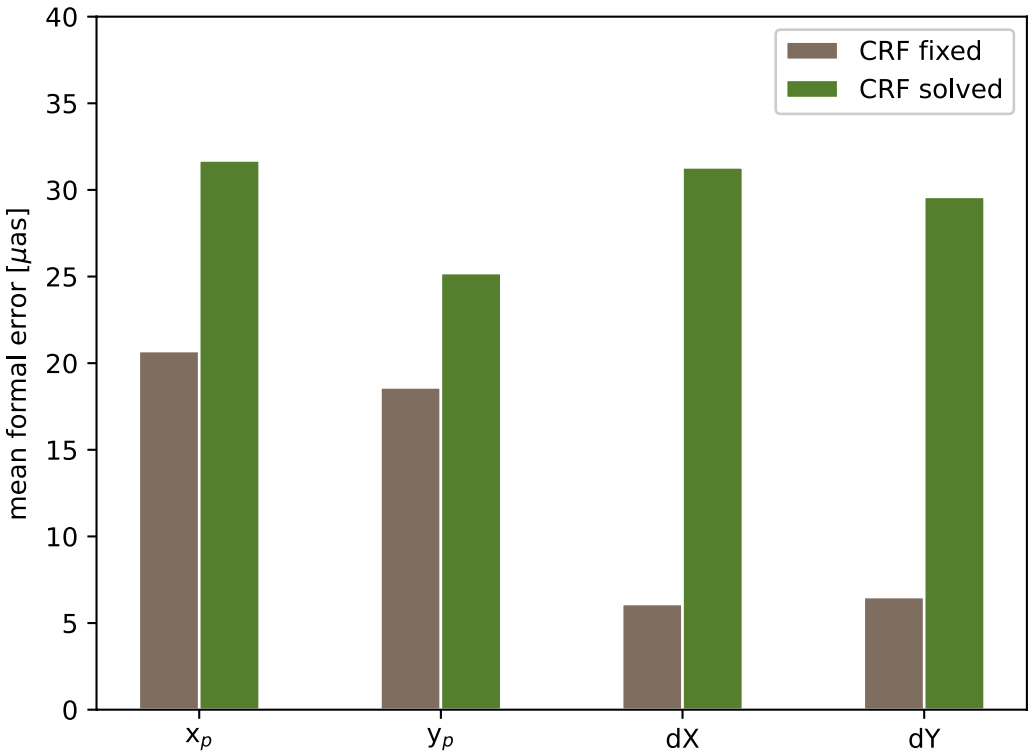

Fig. 2 Nutation and polar motion mean formal errors when **a** fixing (brown, S1) and **b** estimating (green, A1) source coordinates

the accuracy of our estimates, and that the precision is reasonably reflected in the formal errors. The resulting formal errors are presented in Fig. 3, and we can see that the polar motion components match up quite well. The nutation components still show a factor of 2 increase in formal error compared to when sources are fixed to ICRF3, however, we chose not to tighten further the constraint out of concern for practically fixing them to their a priori values. A weighted-mean of the radio source estimates is subsequently calculated (VA-ICRF3), which is then used as a priori for solution S2. The mean biases for this case are shown in Fig. 6. We find that this treatment has aligned nutation to a level of ±5 μas with respect to its a priori mean. We therefore choose to use this VA-ICRF3 for the rest of our analyses.

To make sure that imposing such constraints does not introduce a bias in the NNR condition for the CRF, which is a concern noted by Jacobs et al. (2010), we calculated the rotational and drift components of the VA-ICRF3 with respect to the ICRF3, using the process described in Lambert (2014). We also computed an equivalent transformation between ICRF3 and a VGOS-adjusted ICRF3 from the solution A1, and the results are presented in Tab. 3. The stability of our estimates, calculated as the root mean squared metric of the uncertainties, is on the level of 50 μas, which is reasonably close to the values presented by Lambert (2014) for solutions that use approximately 200 sources to provide a CRF definition. The calculated datum-defining parameters give valuable further insight into how radio sources might be behaving with respect to the VGOS observing bands. We can see, e.g., that imposing constraints on nutation and polar motion is attenuating the estimated transformation parameters which otherwise reach levels up to 32 μas in rotation, and 35 μas in drift. This attenuation is true for all parameters except for the declination bias, B_δ, which remains consistently above 20 μas to the imposing of such constraints. A possible explanation is the geometry of the VGOS network, which for the first three years of operation lacked stations in the southern hemisphere and featured less observations of sources with negative declination. We elaborate on this in Fig. 4 by generating plots of the weighted root-mean square (WRMS) of the radio source position corrections for the right ascension and declination with respect to the declination angle of the radio sources. We find a clear dependence between the WRMS of the declination correction, and the declination angle of the observed source. In particular, for the maximum negative declination of – 40 degrees, the WRMS reaches up to 2—2.5 mas, whereas it drops to 0.1 mas for the maximum positive declination of 80 degrees. This

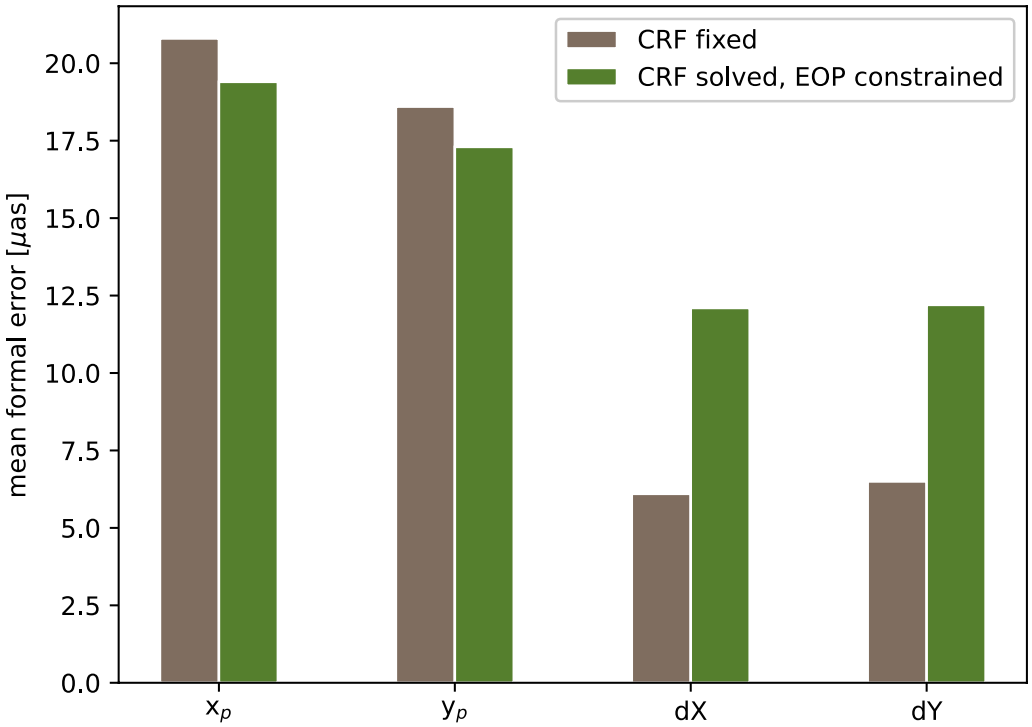

Fig. 3 Nutation and polar motion mean formal errors when **a** fixing (brown, S1) and **b** estimating with constraints on nutation and polar motion (green, A2) source coordinates

effect is almost eliminated for the right ascension, where the estimates fall within the 0.1−0.5 level.

These findings, which coincide with Glomsda et al. (2023), show that an inherent limiting factor of the VGOS network during the first 3 years of observations has indeed been the lack of observing stations at the southern hemisphere. Additionally, the elimination of the rotational and drift components of the datum-defining parameters when generating the VA-ICRF3 through the imposing of EOP constraints, as seen in Table 3, is strongly indicating the crosstalk between EOP and source coordinates. We should note, however, that the precision of our VGOS-adjusted ICRF3 products is limited, as shown by the stability measure, and thus their evaluation on the results level is providing the necessary additional validation. We expect that when more stations become operational, observation cadence increases, and with global solutions which stack observations from multiple 24 h sessions to determine the position of radio sources, this issue will be tackled more rigorously than the method we employ here.

EOP repeatabilities

We already noticed that introducing the VA-ICRF3 eliminates the mean biases for the nutation parameters and significantly reduces them for the polar motion estimates. This is an indication of possible frequency dependence of the radio source positions. If not accounted for, this manifests both in terms of increased WRMS and mean biases. Our decision to create and use the VA-ICRF3 catalogue is having a positive effect on our mean estimates, i.e., as far as accuracy is concerned. However, this is not the case to the same extent for our WRMS, as shown in Fig. 7. The biggest improvement of around 20 % is seen in the Y axis of the celestial pole offset where the updated solution is at the level of 140 μas, followed by the polar motion components which improve by up to 10 %, at the level of 230 μas each. These levels for the WRMS are still fairly large compared to what we expect from the VGOS simulations (Nilsson et al. 2023). The WRMS might be related to how well the CRF is approximated by the sources present on a session-level basis. The stochastic modelling for nutation/polar motion is employed as a second measure, creating the S3 solution setup discussed in section *Parameterization*. The mean formal errors are presented in Fig. 8, where S2 and S3 are reasonably close, which is to be expected as this was the calibration target. The WRMS is plotted in Fig. 9. We detect a notable improvement of 50–60 % in all EOP components. The nutation components are within the 60–80 μas range and polar motion is at the 100–130 μas level. The improvement we detect falls in line to what was presented before regarding

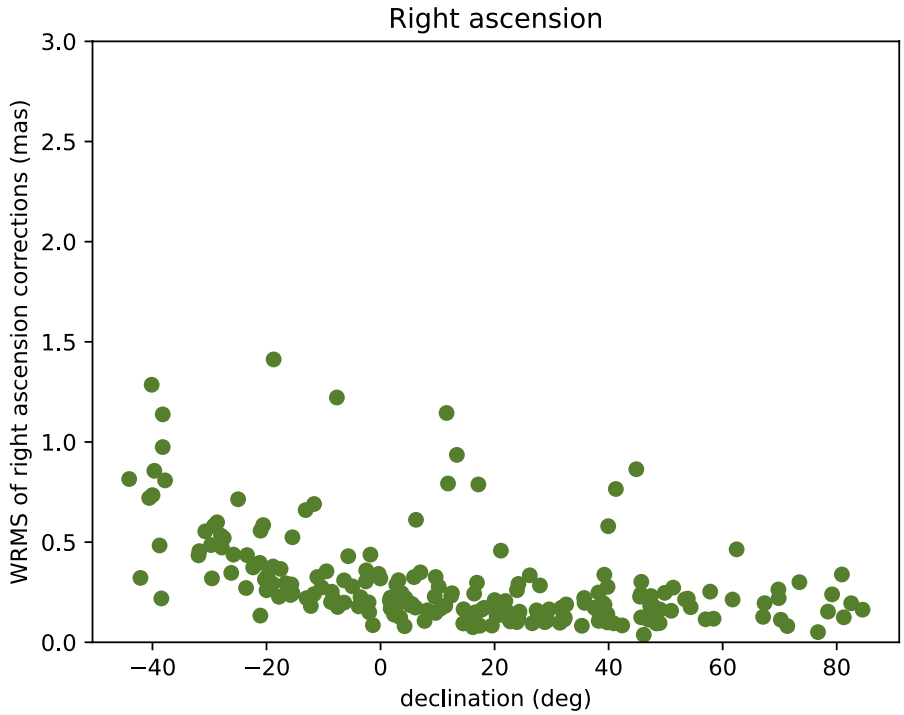

(a)

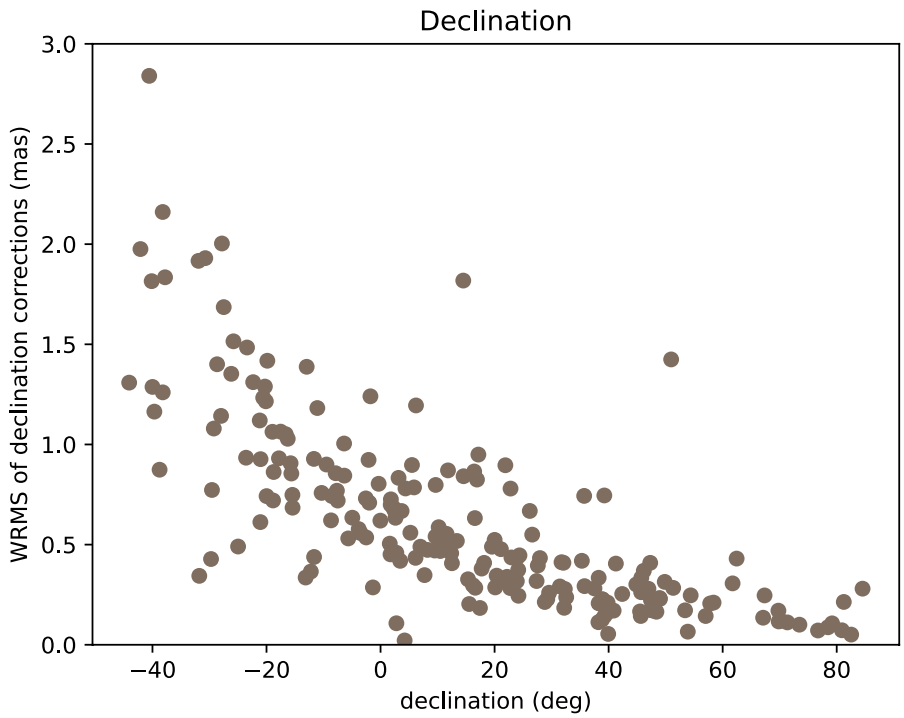

(b)

Fig. 4 The WRMS of the right ascension (green, top) and declination corrections (brown, bottom), with respect to the declination angle of the observed radio sources taken from solution A2

Table 3 Rotational, drift and bias components of the transformation between the ICRF3 catalogues and ICRF3-derived catalogues that have incorporated VGOS observations, in the case of (a) unconstrained (A1), and (b) constrained solution (A2) (in parentheses) with respect to nutation and polar motion. The estimates are given in μas except for D_α and D_δ where they are in μas/rad

Transformation parameters											
$A1$	±	$A2$	±	$A3$	±	D_α	±	D_δ	±	B_δ	±
– 27.9	28.8	– 12.0	31.5	– 32.5	28.8	– 38.7	55.1	– 30.3	63.9	48.3	62.6
(– 0.7)	(27.2)	(– 1.3)	(29.6)	(– 17.9)	(31.6)	(– 7.6)	(55.6)	(– 17.5)	(62.6)	(46.4)	(66.1)

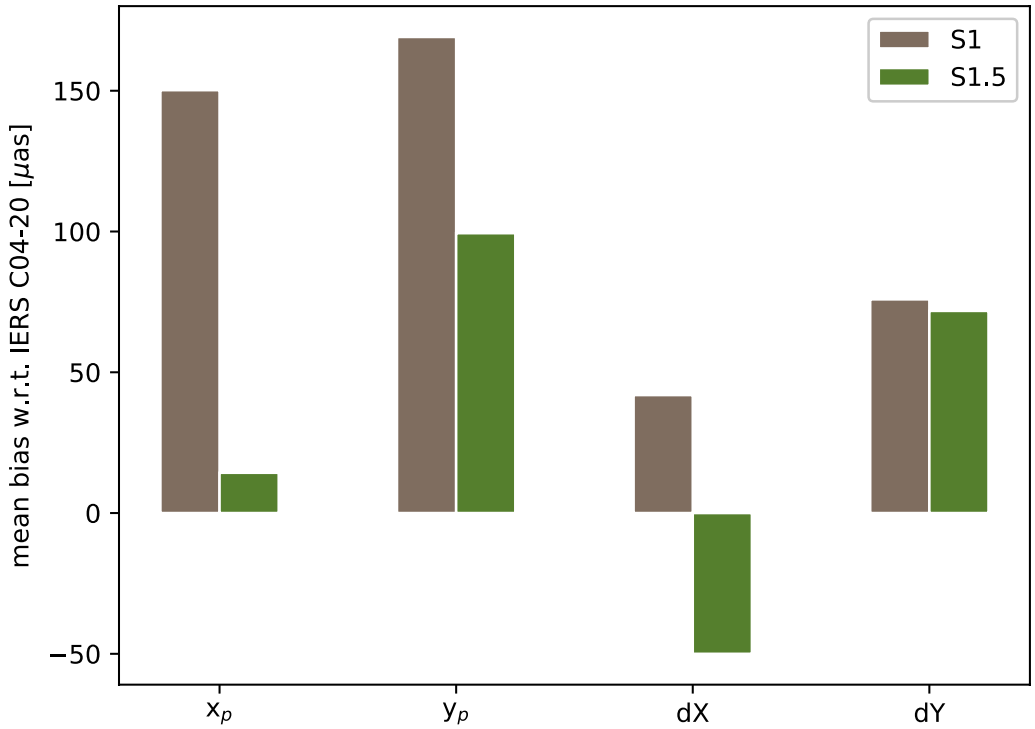

Fig. 5 The mean biases for nutation and polar motion estimates when fixing the sources to ICRF3 (S1) and a VGOS-adjusted ICRF3 (S1.5)

treating EOP with a random walk model (Karbon et al. 2017). In this case, however, we are not determining the stochastic noise of the EOP in terms of an underlying physical process detected and extracted with GNSS as was the case in Karbon et al. (2017). Instead, to mitigate the limited precision of the VA-ICRF3 catalogue that we constructed using only these 72 sessions, we used the formal errors, which is the most consistent performance metric we have at our disposal, to calibrate our filter.

Station position and baseline length repeatabilities

An empirical tuning of a kalman filter always introduces the danger of making a tautological argument, where the result is validating an a priori assumption. In order to see whether we are able to extract better geodetic products in general, we calculated station position and baseline length repeatabilities for solutions S1, S2 and S3 and we present the results in Table 4. We can see a stepwise function in the way that the metrics evolve from one solution to the next. Utilizing the VA-ICRF3, as we already saw in Figs. 6, 7, has the biggest positive effect on the mean biases that are estimated, but not on the WRMS. This is nicely reflected in solution S2, by the fact that the precision is not changed in the station-wise components (north, east, up) but instead in the baseline lengths (bl), indicating an increase in accuracy. Then in solution S3, the stochastic modelling of the EOP allows us to enhance the station-specific precision. At this point we should note, that while north and up components, and baseline lengths are improved by 0.61, 0.38 and 0.31 mm, respectively, from solutions S1 to S3, the east component shows only a marginal improvement. We are investigating possible causes for it. For the best solution we obtained, the repeatabilities that we calculated for the VGOS network

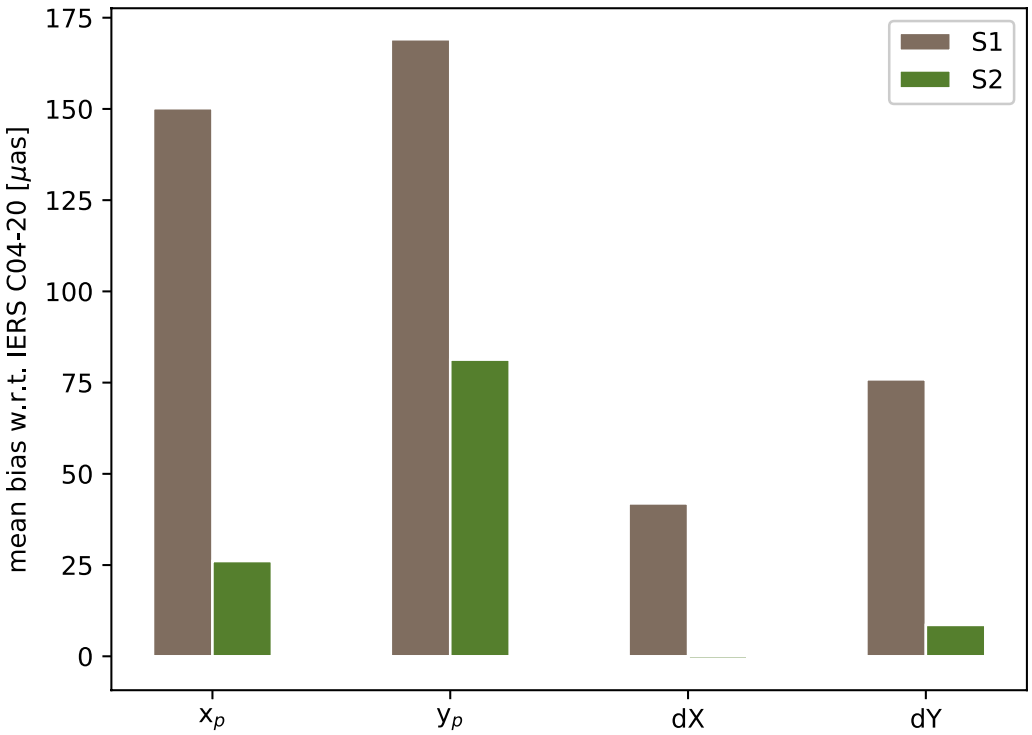

Fig. 6 The mean biases for nutation and polar motion estimates when fixing the sources to ICRF3 (S1) and the VA-ICRF3 (S2). The mean bias of celestial pole offset in the X axis is −0.8 μas in the second case and not easily discernible in the figure

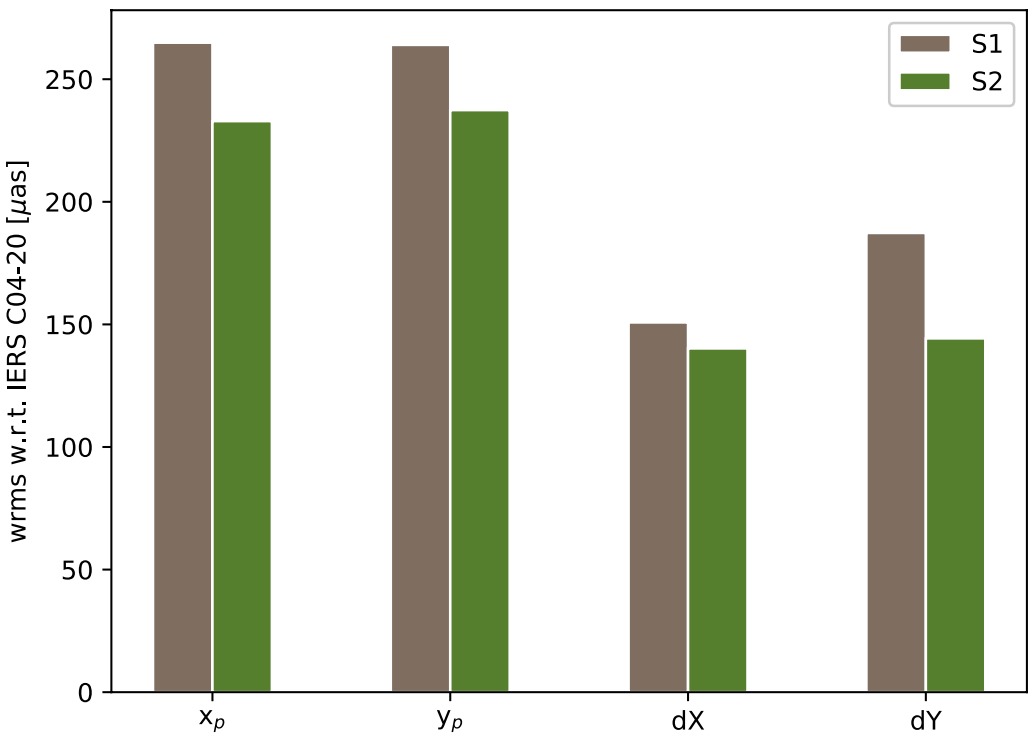

Fig. 7 The WRMS for nutation and polar motion estimates when fixing the sources to ICRF3 (S1) and the VA-ICRF3 (S2)

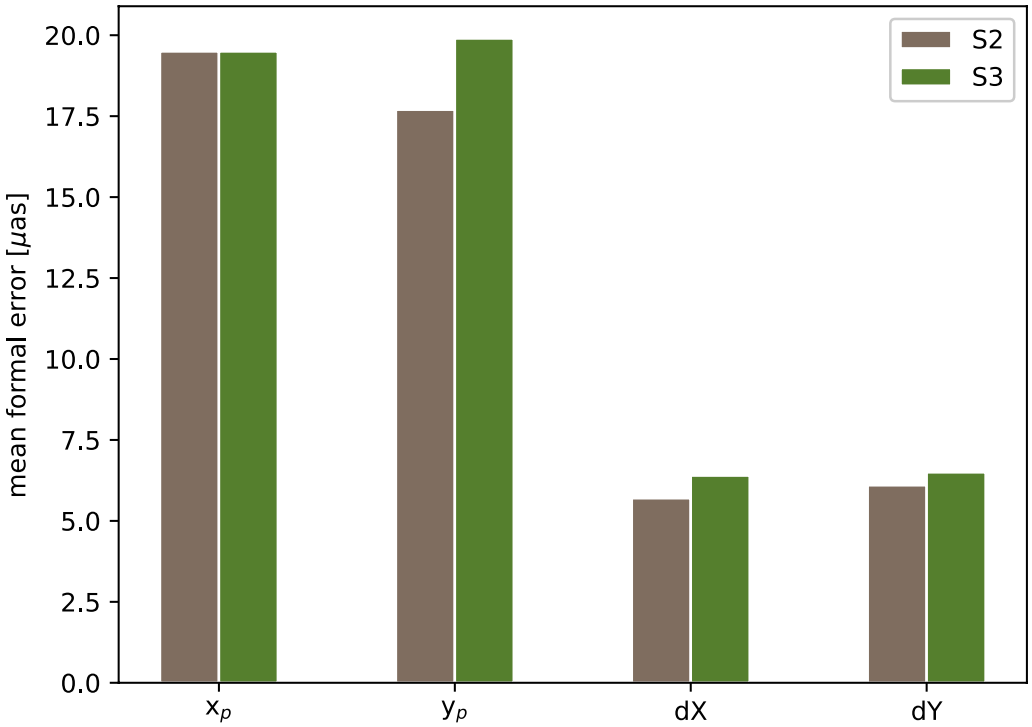

Fig. 8 The mean formal error for nutation and polar motion estimates when treated as constant offsets (S2), and as a random walk (S3)

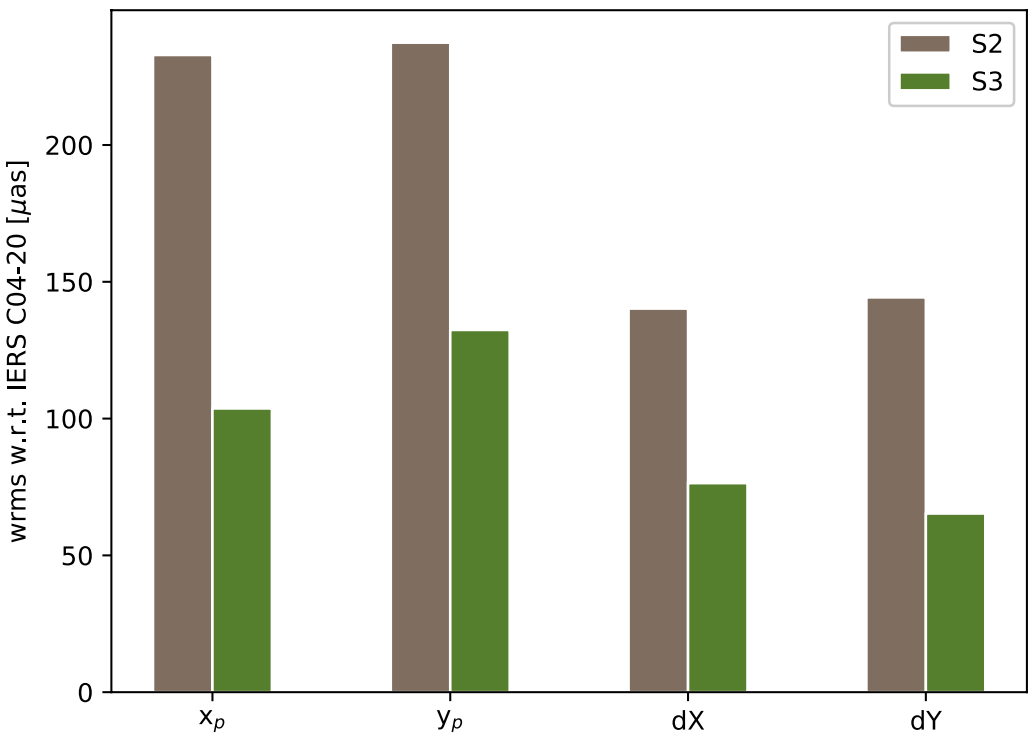

Fig. 9 The WRMS for nutation and polar motion estimates when treated as constant offsets (S2), and as a random walk (S3)

Table 4 The station position repeatabilities in north, east and up, and the baseline length repeatabilities (bl) in mm for solutions S1, S2, S3. The value for bl is calculated at 6000 km

[mm]	North	East	Up	bl
S1	2.66	1.85	4.30	4.58
S2	2.71	1.96	4.36	4.25
S3	2.12	1.80	3.98	4.22

are 1.80 and 2.12 mm for the east and north components and 3.98 mm for the vertical, while the baseline length repeatabilities are 4.22 mm at 6000 km. These results are on the same level to those of analyses using the same dataset see, e.g., Nilsson et al. (2023). The time-series of estimated EOP, the plots for baseline length repeatabilities, and the VA-ICRF3 are included as supplementary material.

Conclusions

In this paper, we investigated the first three years of VGOS 24 h sessions. The station position repeatabilities are 1.80 and 2.12 mm for the east and north components and 3.98 mm for the vertical component. The EOP repeatabilities, however, are considerably above the 40–60 μas level we would expect from VGOS. These results coincide with other studies on this topic which compare also to S/X data (Nilsson et al. 2023; Glomsda et al. 2023). We investigated whether the EOP repeatabilities are related to the CRF definition. More specifically, we constructed a VGOS-adjusted ICRF3 catalogue by favoring source coordinate over EOP corrections in the estimation process. This is done by applying a soft constraint to nutation and polar motion. This constraint showed to have no effect degrading the NNR condition, but on the contrary attenuated the rotational and drift components of the VA-ICRF3 with respect to ICRF3, mitigating possible crosstalk between EOP and radio source coordinates. The declination bias was unaffected by this procedure because it is related to the VGOS network geometry, and in this case it is illustrating the lack of stations in the southern hemisphere. This point was made clearer when looking at the individual radio source position estimates, where those with a negative declination had significantly larger WRMS than those with a positive one.

We proceeded to use this VA-ICRF3 and found that it significantly decreases the mean biases that are estimated with respect to the C04-20 EOP series. We additionally applied an empirically tuned kalman filter that decreased the WRMS of the EOP estimates by approximately 50–60 %. We finally validated that we arrived at a better solution than before, by looking into station position and baseline length repeatabilities, and detecting an improvement in both on the level of 0.3–0.5 mm for all but the east component. The stochastic constraint we input in our KF solution for nutation and polar motion is mitigating some of the CRF related effects. A more rigorous treatment would require the generation of a VGOS-adjusted CRF product in a global solution, or the examination of the effect that VGOS stations in the southern hemisphere have on the EOP estimates.

These results reflect insights that we gained from the first 3 years of VGOS observations. The station position estimates seem to be well on their way to achieving mm-level precision. In the case of EOP, the capability of reaching precision on the 40–50 μas is attainable. However, further studies need to be done, along with the ever-growing network of VGOS stations and the increasing observation cadence, to identify optimal estimation and handling methods of the VGOS data that will deliver geodetic products of utmost precision and accuracy.

Author contributions

PKD designed the study, implemented the necessary extensions in the analysis software, analysed the data, interpreted the results, prepared all graphical material, and wrote the manuscript. RH supervised the work and supported the result interpretation as well as writing of the manuscript. All authors read and approved the final manuscript.

Funding

Open access funding provided by Chalmers University of Technology. This work is supported by Rymdstyrelsen, the Swedish National Space Agency.

Availability of data and materials

All used VLBI data are publically available via the international VLBI Service for Geodesy and Astrometry (IVS).

Declarations

Competing interests

The authors declare that there are no competing interests.

Received: 12 December 2022 Accepted: 10 July 2023
Published online: 19 July 2023

References

Altamimi Z, Rebischung P, Collilieux X, Métivier L, Chanard K (2023) Itrf 2020: An augmented reference frame refining the modeling of nonlinear station motions. J Geodesy 97(5):47

Bolotin S, Baver K, Gipson J, Gordon D, MacMillan D (2015) Implementation of the vgosdb format. In: Rüdiger Haas, and Francisco Colomer (Eds.), Proceedings of the 22nd European VLBI Group for Geodesy and Astrometry Working Meeting, Ponta Delgada, Azores, pp 150–152

Chang G (2014) Robust kalman filtering based on mahalanobis distance as outlier judging criterion. J Geodesy 88(4):391–401. https://doi.org/10.1007/s00190-013-0690-8

Charlot P, Jacobs C, Gordon D, Lambert S, De Witt A, Böhm J, Fey A, Heinkelmann R, Skurikhina E, Titov O et al (2020) The third realization of the international celestial reference frame by very long baseline interferometry. Astron Astrophys 644:A159

de Witt A, Charlot P, Gordon D, Jacobs CS (2022) Overview and status of the international celestial reference frame as realized by VLBI. Universe 8(7):374
Diamantidis PK, Haas R, Varenius E, Schartner M, Matsumoto S (2022) Combining VGOS, legacy S/X and GNSS for the determination of UT1. J Geodesy 96(8):1–12
Elosegui P, Barrett J, Corey BE, Niell AE, Ruszczyk CA, Titus MA, Bolotin S, Gipson JM, Himwich WE, Neidhart A, et al. (2018) An evaluation of VGOS data, precision, and accuracy. In: Abstracts of the AGU Fall Meeting, Washington, D.C., vol 2018, pp G33A–05
Glomsda M, Seitz M, Angermann D (2023) Comparison of simultaneous VGOS and legacy VLBI sessions. In: Kyla L. Armstrong, Dirk Behrend, and Karen D. Baver (Eds.), IVS 2022 General Meeting Proceedings, Online, pp 187–191
Haas R, Varenius E, Matsumoto S, Schartner M (2021) Observing UT1-UTC with VGOS. Earth Planets Space 73(1):1–7. https://doi.org/10.48550/arXiv.2011.14975
Herring TA, Davis JL, Shapiro II (1990) Geodesy by radio interferometry: The application of Kalman Filtering to the analysis of very long baseline interferometry data. J Geophys Res Solid Earth. 95(B8):12,561–12,581, https://doi.org/10.1029/JB095iB08p12561
Hobiger T, Otsubo T (2014) Combination of GPS and VLBI on the observation level during CONT11–common parameters, ties and inter-technique biases. J Geodesy 88(11):1017–1028. https://doi.org/10.1007/s00190-014-0740-x
Hobiger T, Otsubo T (2017) Combination of space geodetic techniques on the observation level with c5++: common nuisance parameters and data weighting. In: van Dam T (ed) REFAG 2014. Springer International Publishing, Cham, pp 31–37
Hobiger T, Otsubo T, Sekido M, Gotoh T, Kubooka T, Takiguchi H (2010) Fully automated VLBI analysis with c5++ for ultra rapid determination of UT1. Earth Planets Space 62(12):933–937. https://doi.org/10.5047/eps.2010.11.008
Hobiger T, Otsubo T, Sekido M (2014) Observation level combination of SLR and VLBI with c5++: a case study for TIGO. Advances in Space Research 53(1):119–129. https://doi.org/10.1016/j.asr.2013.10.004, https://www.sciencedirect.com/science/article/pii/S0273117713006388
Jacobs CS, Heflin M, Lanyi G, Sovers O, Steppe J (2010) Rotational alignment altered by source position correlations. In: Behrend Dirk, Baver Karen D (eds) IVS 2010 general meeting proceedings. Hobart, Australia, pp 305–309
Karbon M, Soja B, Nilsson T, Deng Z, Heinkelmann R, Schuh H (2017) Earth orientation parameters from VLBI determined with a Kalman filter. Geodesy Geodyn 8(6):396–407
Koch KR (1988) Parameter estimation and hypothesis testing in linear models. Springer-Verlag, Berlin, Heidelberg
Lambert S (2014) Comparison of VLBI radio source catalogs. Astron Astrophys 570:A108
Landskron D, Böhm J (2018) VMF3/GPT3: refined discrete and empirical troposphere mapping functions. J Geodesy 92(4):349–360
Mikschi M, Böhm J, Schartner M (2021) Unconstrained estimation of VLBI global observing system station coordinates. Adv Geosci 55:23–31
Niell A, Barrett J, Burns A, Cappallo R, Corey B, Derome M, Eckert C, Elosegui P, McWhirter R, Poirier M et al (2018) Demonstration of a broadband very long baseline interferometer system: a new instrument for high-precision space geodesy. Radio Sci 53(10):1269–1291
Nilsson T, Soja B, Karbon M, Heinkelmann R, Schuh H (2015) Application of Kalman filtering in VLBI data analysis. Earth Planets Space 67(1):136. https://doi.org/10.1186/s40623-015-0307-y
Nilsson T, Haas R, Varenius E (2023) The Current and Future Performance of VGOS. In: Behrend D, Baver KD, Armstrong KL (eds) IVS 2022 General Meeting Proceedings, Online, pp 192–196
Noll CE (2010) The crustal dynamics data information system: a resource to support scientific analysis using space geodesy. Adv Space Res 45(12):1421–1440
Park P, Kailath T (1995) New square-root algorithms for kalman filtering. IEEE Trans Autom Control 40(5):895–899. https://doi.org/10.1109/9.384225
Pearlman M, Appleby G, Behrend D, Bergstrand S, Donovan H, Emerson C, Esper J, Hase H, Long J, Ma C, McCormick D, Noll C, Pavlis E, Ferrage P, Saunier J, Stowers D, Wetzel S (2015) GGOS requirements for core sites. https://cddis.nasa.gov/docs/2015/SiteRecDoc_Rev2_D3.4.pdf
Plag HP, Rothacher M, Pearlman M, Neilan R, Ma C (2009) The global geodetic observing system. In: Advances in geosciences: Volume 13: Solid Earth (SE), World Scientific, pp 105–127
Ribeiro MI (2004) Kalman and extended kalman filters: concept, derivation and properties. Inst Syst Robot 43(46):3736–3741
Soja B, Nilsson T, Karbon M, Zus F, Dick G, Deng Z, Wickert J, Heinkelmann R, Schuh H (2015) Tropospheric delay determination by Kalman filtering VLBI data. Earth Planets Space 67(1):144. https://doi.org/10.1186/s40623-015-0293-0
Sovers OJ, Jacobs CS, Lanyi GE (2004) MODEST: a tool for geodesy and astrometry. In: Vandenberg Nancy, Baver Karen D (eds) IVS 2004 General Meeting Proceedings. Canada, Ottawa, pp 272–276
UN (2015) A global geodetic reference frame for sustainable development. https://www.un.org/ga/search/view_doc.asp?symbol=A/69/L.53
Varenius E, Haas R, Nilsson T (2021) Short-baseline interferometry local-tie experiments at the Onsala space observatory. J Geodesy 95(5):1–21
Webb F, Zumberge J (1995) An introduction to GIPSY/OASIS II, JPL D-11088. Jet Propulsion Laboratory, Pasadena
Xu MH, Savolainen T, Anderson JM, Kareinen N, Zubko N, Lunz S, Schuh H (2022) Impact of the image alignment over frequency for the vlbi global observing system. Astron Astrophys 663:A83

Publisher's Note

Periklis-Konstantinos Diamantidis Is a Ph.D. student supported by Rymdstyrelsen, the Swedish National Space Agency, under project324 number 166/16.